



HAL
open science

Analysis and comparison of transonic buffet phenomenon over several 3D wings

Edoardo Paladini, Julien Dandois, Denis Sipp, Jean-Christophe Robinet

► **To cite this version:**

Edoardo Paladini, Julien Dandois, Denis Sipp, Jean-Christophe Robinet. Analysis and comparison of transonic buffet phenomenon over several 3D wings. *AIAA Journal*, 2018, pp.1-18. 10.2514/1.J056473 . hal-02464839v2

HAL Id: hal-02464839

<https://hal.science/hal-02464839v2>

Submitted on 1 Mar 2019

HAL is a multi-disciplinary open access archive for the deposit and dissemination of scientific research documents, whether they are published or not. The documents may come from teaching and research institutions in France or abroad, or from public or private research centers.

L'archive ouverte pluridisciplinaire **HAL**, est destinée au dépôt et à la diffusion de documents scientifiques de niveau recherche, publiés ou non, émanant des établissements d'enseignement et de recherche français ou étrangers, des laboratoires publics ou privés.

Analysis and comparison of transonic buffet phenomenon over several 3D wings

E. Paladini¹, J. Dandois², D. Sipp³
ONERA, The French Aerospace Lab, 92190 Meudon, France

and

J.-Ch. Robinet⁴
DynFluid Laboratory, Arts et Métiers ParisTech, 75013 Paris, France

The transonic buffet is a complex aerodynamic instability which appears on wings and airfoils at high subsonic Mach number and/or angle of attack. It consists in a shock oscillation that implies pressure and notably lift fluctuations, thus limiting the flight envelope of civil aircrafts. The aim of the present paper is to improve the understanding of the flow physics of the 3D transonic buffet over swept wings through the analysis and comparison of four different experimental databases, and in particular identifying characteristic values of the buffet phenomenon such as Strouhal numbers, convection velocities, buffet onset etc. It is shown that some non-dimensionalized numbers are kept constant between the different databases and consequently can be considered as characteristics of the 3D buffet, whereas others change. The key to understanding the transonic buffet phenomenon lies in explaining the common features but also the variability of transonic buffet parameters in different configurations. In particular, it is shown that the 3D buffet is characterized by a Strouhal number in the range 0.2-0.3 and a spanwise convection velocity of $0.245 \pm 0.015 U_\infty$, where U_∞ denotes the freestream velocity. These characteristic ranges of values are much larger those of the 2D buffet phenomenon, which suggests different physical explanations.

¹ PhD Student, Department of Aerodynamics, Aeroelasticity and Acoustics, edoardo.paladini@onera.fr.

² Ph.D. Eng, Department of Aerodynamics, Aeroelasticity and Acoustics, julien.dandois@onera.fr.

³ Professor, Department of Aerodynamics, Aeroelasticity and Acoustics, denis.sipp@onera.fr.

⁴ Professor, DynFluid Laboratory, Arts et Métiers ParisTech, Jean-Christophe.Robinet@ensam.eu.

Nomenclature

α	= Angle of attack, <i>deg</i>
b	= Wingspan, <i>m</i>
c	= Local chord length, <i>m</i>
MAC	= Mean aerodynamic chord, <i>m</i>
f	= Frequency, <i>Hz</i>
k	= Wavenumber, m^{-1}
λ	= Wavelength, <i>m</i>
a	= Speed of sound, $m.s^{-1}$
x, y, z	= Streamwise, spanwise and wall-normal spatial coordinates
Re_{MAC}	= Reynolds number based on the mean aerodynamic chord
U_∞	= Freestream velocity, $m.s^{-1}$
U_g	= Group velocity, $m.s^{-1}$
U_p	= Phase velocity, $m.s^{-1}$
$M = U/a$	= Mach number
L	= Characteristic length, <i>m</i>
$St = fL/U_\infty$	= Strouhal number
U_c	= Convection velocity, $m.s^{-1}$
Λ	= Wing sweep angle, <i>deg</i>
β	= Convection velocity angle, <i>deg</i>

I. Introduction

On civil aircrafts, during cruise flight, a shock wave is present on the upper side of the wing. If the Mach number and/or the angle of attack are increased beyond a limit, a separation appears downstream of the shock. This separation leads to an instability of the shock wave boundary layer interaction called transonic buffet. The shock position starts to oscillate in synchronisation with

the detachment-reattachment of the boundary layer, which results in large pressure fluctuations. If coupled with a structural mode, integral aerodynamic forces and moments fluctuations lead to structural vibrations of the entire wing, called buffeting. These vibrations can weaken the structure of the wings and in the worst case bring to a crash by fatigue. Consequently the buffet phenomenon limits the flight envelope of civil aircrafts. So it is interesting to get a deeper understanding of the buffet phenomenon to better predict its onset. Delaying the values of Mach number (M) and angle of attack (α) for which buffet onset occurs would lead to an improvement of aircraft aerodynamic performance (increase of the maximum take-off weight, range, decrease of the wing area etc). During the wing design phase of an aircraft, buffet onset is evaluated just by empirical criteria (kink on the lift curve, divergence of the trailing edge pressure, etc.) and the experience coming from previous aircraft. In particular, the knowledge of the unsteady loads is a crucial point. Wind tunnel tests on models at atmospheric conditions are generally not fully realistic because of the smaller Reynolds number, while the flight tests are complete but available too late and too expensive. This is the reason why computational fluid dynamics is gaining increasing importance with Unsteady RANS (Reynolds Averaged Navier-Stokes closed with a turbulence model) simulations or more evolved Hybrid RANS/LES methods.

The first studies on buffet were conducted during and after World War II, when thanks to technology evolution aircrafts reached transonic velocities. The aeronautical community already spoke about buffeting, referring to it as an aero-elastic problem. But only in these years the community found out the cause of one kind of buffeting (at transonic velocities) in an instability of the shock-boundary layer interaction and called it transonic buffet. They started performing tests in order to better understand the phenomenon, prevent structural damage and eventually crash. Precisely the tests were more focused on control than on the understanding of the instability. That is the reason why the first works really devoted to the understanding of the buffet physics arrived only later and were first focus on 2D airfoils. Today the phenomenon is not completely understood but there are two main physical mechanisms to explain 2D buffet. The first proposed by Lee [1] consists in a self-sustained loop based on the coupling between the shock and the trailing edge (TE)

through pressure waves (see figure 1).

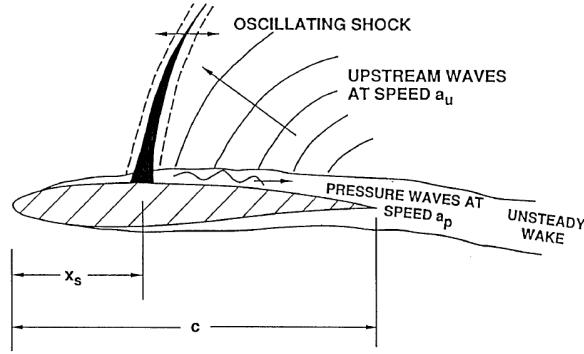


Fig. 1: Model of self-sustained shock oscillations. X_s : shock position, c : chord from [1].

The shock wave generates pressure waves which propagate downstream inside the boundary layer; these waves are scattered at the TE, generating waves that travel upstream back towards the shock outside the boundary layer. These waves create new pressure waves and close the loop of the self-sustained model. Deck [2] and Memmolo et al. [3] suggest (based on numerical studies) that the waves propagating downstream are of hydrodynamic nature while those propagating upstream are acoustic. Memmolo precisely describes all the possible acoustic rays displaying the right frequency and which are emitted at the trailing edge and hit the shock front halfway of the sonic line. Deck [2] and Xiao et al. [4] evaluated the propagation time from the shock wave to the TE, which well agreed with the experimental value. The path of the closed-loop model is not completely established, in some cases upstream pressure waves are visualized even on the lower side of the airfoil (Jacquin et al. [5]) which suggests a different path for the closed-loop. The second physical explanation is the stability analysis by Crouch et al. [6], where the shock instability is explained through an unstable global mode. Unstable global modes are generated by a self-sustained process as well but here the pressure fluctuations appear downstream of the shock base and move upward round the shock, while spreading a little towards the trailing edge (TE) [7]. This kind of stability analysis has been repeated by Sartor et al. [8] and Guiho [9]. The results show a good agreement on the values of buffet frequency and yield a precise description of the buffet phenomenon at different M - α values: the buffet onset, the well-established buffet and the buffet exit. Memmolo et al. [3], after proposing a path for the Lee-model consistent with the frequency of buffet, performed a

filtering of the acoustic field and showed that the buffet instability is either highly localized around the shock or connected with the separation bubble dynamics. Recently Timme & Thormann [10] performed a 3D global stability analysis, an approach similar to Crouch et al. [6], but on an entire half wing/fuselage-body. The emergence of a weakly damped global mode is found in the range $\alpha = 2^\circ\text{-}3^\circ$ but no unstable mode is found yet. Indeed this kind of analysis in 3D is very interesting because it gives the possibility to understand if the 3D transonic buffet phenomenon is due to an unstable global mode like in 2D or if it comes from a different physical nature.

It is however well established that the flow physics between 2D and 3D buffet is different (Reneaux et al. [11], Roos [12], Molton et al. [13] and Dandois [14]). The frequency spectrum of 2D transonic buffet is more a well defined peak (Jacquin et al. [5]) while in 3D, it is more broadband (Roos [12]). The buffet frequency is also much higher in 3D than in 2D, a typical range of Strouhal numbers (based on the mean aerodynamic chord, $St = fL/U_\infty$ with $L = MAC$) in 3D buffet is around 0.2-0.6 while it is around 0.05-0.07 in 2D. This means that the buffet frequencies are 4 to 10 times higher in 3D than in 2D. The amplitude of the shock-oscillation changes as well; even though it is more complicated to define a precise ratio because it depends on the angle of attack, 2D shock-oscillations are about 10 times larger than in 3D. Typical shock oscillation amplitude in 3D is 2% of the chord, while it is 20% in 2D.

Studies conducted over 3D configurations are mainly experimental (Hwang & Pi [15], Roos [12], Eckstrom et al. [16], Destuynder [17], Eckstrom et al. [18], Lutz et al. [19], Dandois [14]). In early studies (Hwang & Pi [15]), the experimental results were more focused on the structural response of the aircraft and the effects at the pilot seat. However some interesting PSD distributions obtained with unsteady pressure transducers have been provided and the first value of buffet frequency is defined (a Strouhal of about 0.23). Roos [12] shows a more complete analysis over a half-wing body configuration with the definition of the frequency range of 3D buffet and a characterization of the bump in the spectra. Even if the phenomenon was far from being understood, some studies of buffet control were performed as well. Destuynder [17] tested a closed-loop control based on

accelerometers and strain gauges as input signals for the flaperons. Only recent studies become more complete and enter more deeply in the 3D buffet physics. Molton et al. [13] presented the results of a test campaign on a half-wing body configuration in the ONERA S3Ch wind tunnel. The Strouhal number was found in the range 0.2-0.6. Dandois [14] performed a complete analysis of two wind tunnel tests on a half-wing body configuration. He gave values for the buffet onset at different values of M - α and characterized the frequency spectra evolution in the chordwise and spanwise directions. By using different signal processing tools, the convection velocities of the buffet phenomenon and of the Kelvin-Helmholtz instability were obtained.

These last years, more and more numerical simulations of 3D configurations have been performed. These simulations give a better overview of the overall three-dimensional flow field, allowing comparison with experimental data and filling the lack of model instrumentation in all the experiments. Unsteady RANS (Sartor & Timme [21], Iovnovich & Raveh [22]) and more expensive Detached-Eddy simulations (DES) (Brunet & Deck [23], Deck et al. [20], Lutz et al. [19], Sartor & Timme [24]) have been performed. Brunet and Deck [23], to the author's knowledge, were the first to perform simulations of the 3D transonic buffet by DES with a well reproduction of the entire flow (figure 2).

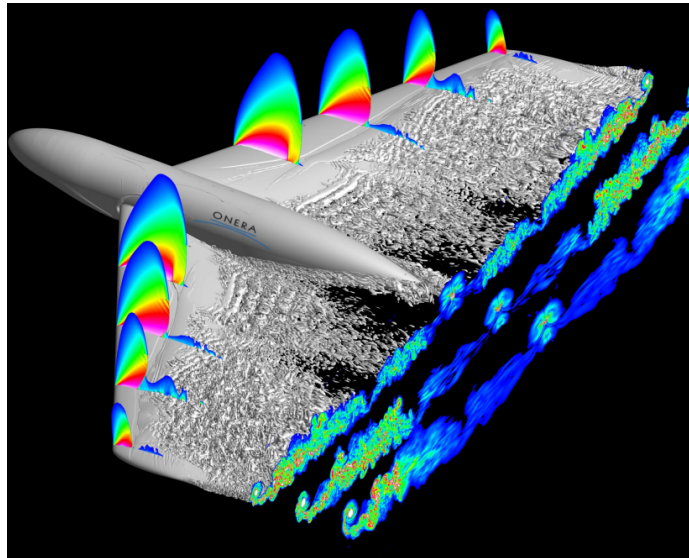


Fig. 2: ZDES simulations of transonic buffet [20].

Lately, Iovnovich & Raveh [22] and Sartor & Timme [21] performed URANS simulations of the transonic buffet. Iovnovich & Raveh [22] studied the phenomenon on 3D wings at different sweep angles and aspect ratio. They were the first to give an interpretation of the path from 2D to 3D buffet. At zero or small sweep angles the results are similar to the 2D phenomenon, while when the sweep is increased, the Strouhal number increases too and reaches typical values of the 3D phenomenon with spanwise-propagating waves appearing on the wing, called “buffet cells”. In the following years this convective phenomenon was also found experimentally, Dandois [14] compute the convection velocity of these “buffet cells” by using a cross-spectrum analysis in the spanwise direction. These buffet cells are typical of the 3D transonic buffet. Sartor & Timme et al.[21] as well found the complex structures in the spanwise direction typical of the 3D buffet. They studied the effects of different parameters such as Mach number, angle of attack and turbulence model on URANS simulations and in ref. [24], they showed a comparison with a delayed-DES simulation: even though DDES shows obviously a deeper description of the flow, a good agreement of the main features of the flow is found. Lutz et al. [19] recently performed a complete experimental study of 3D transonic buffet in the European Transonic Windtunnel and compared with hybrid RANS/LES simulations. He obtained a rather good agreement between numerical and experimental results with a precise description of the unsteady development of the massively separated wing flow. The link between 2D and 3D transonic buffet is a relevant question today, as well as the impact of aerodynamic parameters, such as Mach number, angle of attack, Reynolds number, etc. on different wings. A physical model explaining both kinds of buffet and the transition between them is a challenging objective and the present paper settle the base of this model. The main objective of the present paper is the analysis of the different databases, the definition of the characteristic values of non-dimensional numbers and the study of their sensibility as function of the flow physics or the geometry.

The present paper is a continuation of Molton et al. [13] and Dandois [14] ones. The first is more oriented in the control of the buffet. The second is based on two wind tunnel tests and oriented on the analysis of the phenomenon. Here two new databases are analyzed, further spectral

analyses are performed and objective is more oriented in the variability of the phenomenon.

The paper is organized as follows. Section 2 defines the experimental set-up of each project. First results are given in section 3, starting with the values of buffet onset and continuing in section 4 with a deep analysis of some power spectral densities. In section 5, signal processing tools like cross-spectra and frequency-wavenumber spectra are used to compute convection velocities of the buffet phenomenon. Finally, a synthesis of the results is presented and perspectives are given in the conclusion.

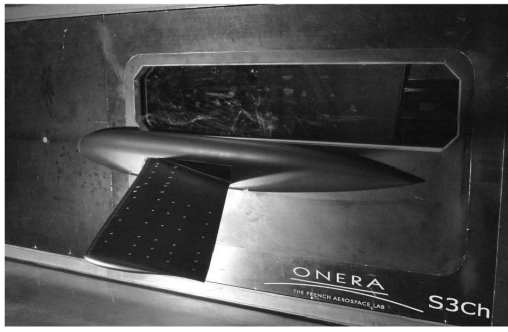
II. Experimental setup

In the present article, four different campaigns are analyzed and compared. These campaigns were performed in three wind-tunnels over four different half wing/fuselage-body models. They correspond to the following projects:

1. an ONERA research project called “BUFET’N Co” launched in 2007 in the ONERA S3Ch wind tunnel over a half wing/fuselage-body based on the OAT15A airfoil (figure 3a).
2. an European project called “AVERT” launched in 2007 in the ONERA S2MA wind tunnel over a half wing/fuselage-body based also on the OAT15A airfoil (figure 3b).
3. a French project called “DTP Tremblement” launched in 2004 in the ONERA S2MA wind tunnel over a half wing/fuselage-body Dassault Aviation model (figure 3c).
4. an European project called “FLIRET” launched in 2005 in the European Transonic Windtunnel (ETW) over a half wing/fuselage-body Airbus model (figure 3d).

Figure 3 shows pictures of the four models inside their corresponding wind-tunnels.

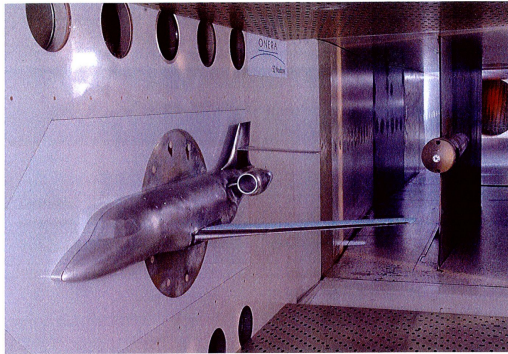
S3Ch is a continuous closed-circuit transonic wind tunnel in the ONERA-Meudon center. The test section size is $0.76\text{ m} \times 0.82\text{ m} \times 2.2\text{ m}$. The stagnation pressure is the atmospheric one, and the stagnation temperature lies between 290 and 310 K . The shapes of the upper and lower walls are adapted for each flow condition based on a steady flow hypothesis so as to reproduce far-field



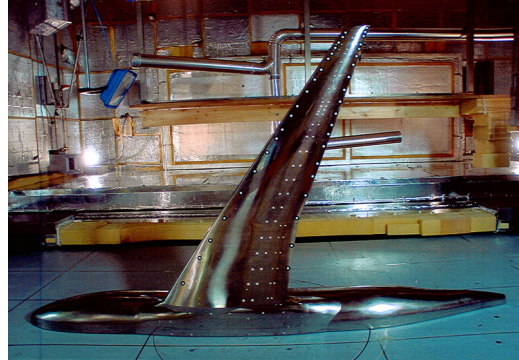
(a) BUFET'N Co model in S3Ch wind tunnel



(b) AVERT model in S2MA wind tunnel.



(c) DTP Tremblement model in S2MA wind tunnel



(d) FLIRET model in ETW.

Fig. 3: Overview of the four models inside their respective wind tunnels

conditions.

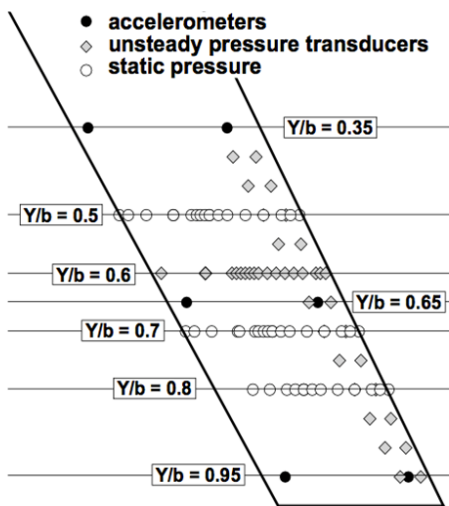
The freestream Mach number M is set at 0.82. The angle of attack of the model can be varied between 2° and 4° by a mechanical system and/or a proper adjustment of the adaptive walls. The model (figure 3a) is composed of a swept wing attached on a half-fuselage, the sweep angle at the leading edge (LE) is 30° and the wing is based on the supercritical OAT15A airfoil. From root to tip, the chord varies between 0.24 and 0.2 m over a span of 0.704 m . The Reynolds number based on the mean aerodynamic chord ($MAC = 0.22 m$) is $Re_{MAC} = 2.5 \times 10^6$. Boundary-layer transition is triggered on the model by using a carborundum strip located at $x/c = 7\%$ on both the upper and lower side of the model, as well as on the fuselage. The model is equipped with 49 static pressure taps, 39 unsteady Kulite pressure transducers, and 6 accelerometers. The acquisition of dynamic data is performed at 20480 Hz. Figure 4a shows the locations of the equipment on the suction side of the wing.

The S2MA wind tunnel of ONERA Modane-Avrieux center is a continuous pressurized subsonic/transonic/supersonic wind tunnel. The test section size is 1.765 m x 1.75 m. Upper and lower walls are perforated in order to reduce their influence on the flow.

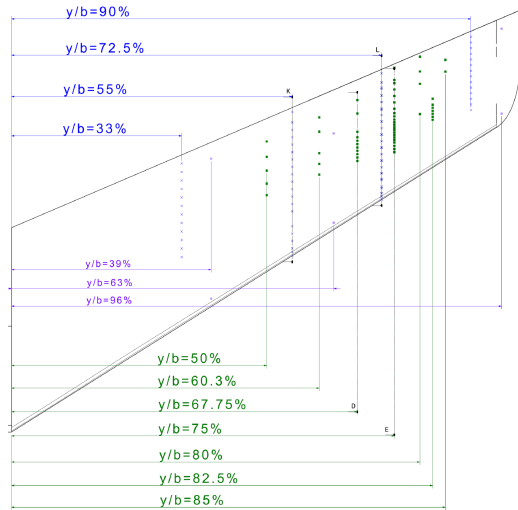
The AVERT model is a simplified half wing/body model. Most of the wing profile is based on the OAT15A airfoil like the BUFET'N Co model. The span of this half model is equal to 1.225 m, the mean aerodynamic chord is equal to 0.3375 m and the sweep angle at the LE is 30°. The chord length is 0.450 m at the wing root and 0.225 m at the wing tip. Tests were performed for different stagnation pressure values (from 0.6 bar up to 1.8 bars) for several freestream Mach numbers between 0.78 and 0.86. The Reynolds numbers investigated range from 2.83×10^6 to 8.49×10^6 (based on the mean aerodynamic chord). Many steady pressure taps and unsteady pressure transducers are installed on the model: 86 pressure taps on 4 wing sections, 65 on the upper and 21 on the lower surface of the wing; 57 unsteady pressure transducers on 7 wing sections, 53 on the upper and 4 on the lower surface of the wing; 3 wing sections with 2 accelerometers each. The acquisition of dynamic data is performed at 2048 Hz. Figure 4b shows the locations of the equipment on the suction side of the wing.

The European Transonic Wind tunnel (ETW) located in Cologne, Germany, is an industrial cryogenic pressurized facility. A pressurized tunnel at very low “cryogenic” temperatures can provide real-flight Reynolds numbers. The ETW has a closed aerodynamic circuit with a test section size of 2 m x 2.4 m x 8.73 m.

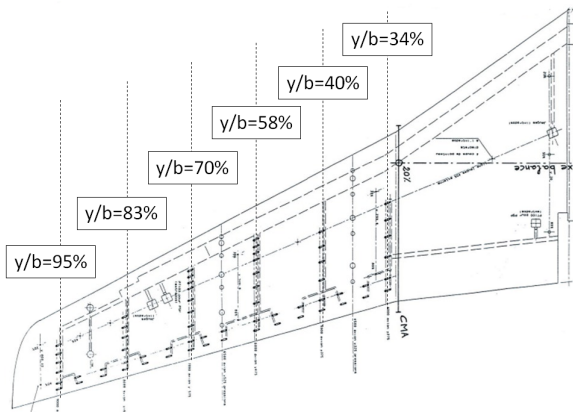
The FLIRET model is a half wing/fuselage-body defined by Airbus UK. It is a typical Airbus model with a supercritical airfoil and a double sweep at the trailing edge. The half span is 1.3167 m, the mean aerodynamic chord is 0.384 m and the sweep angle at the leading edge is 30°. The tests analyzed in this paper are performed with a free transition at different Mach numbers ranging from 0.85 to 0.93. The Reynolds numbers investigated range from 23.5×10^6 to 70.5×10^6 (based on *MAC*). The model is equipped with 42 Kulites and 6 accelerometers (2 on the fuselage and 4 on the wing). Figure 4c shows their locations on the suction side of the wing. The acquisition of dynamic data is performed at 4096 Hz during 16 seconds with a low-pass filter at 819 Hz.



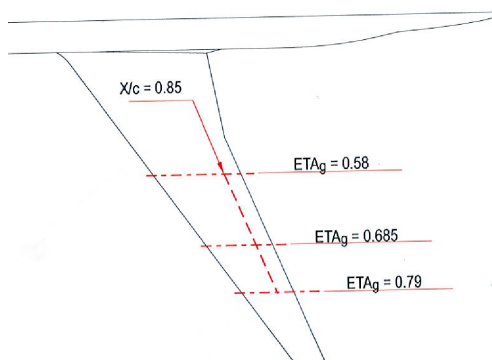
(a) BUFET'N Co



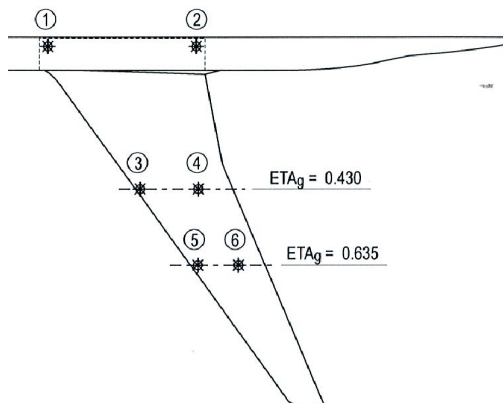
(b) AVERT: in blue static pressure, in green unsteady pressure transducers, in purple accelerometers.



(c) DTP Tremblement: the black points are unsteady pressure transducers.



(d) FLIRET: in red 4 lines of unsteady pressure transducers



(e) FLIRET: in black 6 accelerometers

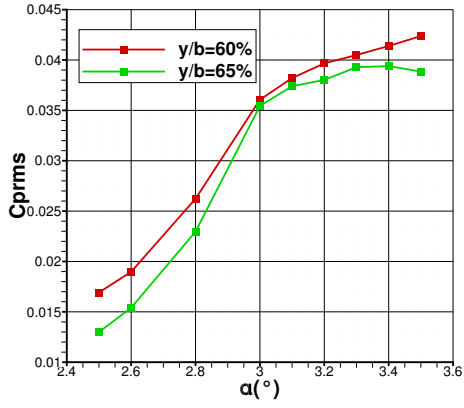
Fig. 4: Models equipment

Finally, the DTP Tremblement model, tested in S2MA as the AVERT model, is a half wing/fuselage-body defined by Dassault Aviation. It is also based on a supercritical airfoil with a double sweep wing. The half span is 0.943 *m* and the mean aerodynamic chord is 0.251 *m*. Boundary-layer transition is triggered on the model by using a carborundum strip located at $x/c = 10\%$ or 24% on the upper side of the wing, at $x/c = 10\%$ on the lower side of the wing. The tests analyzed in this paper are performed at different values of the Mach number between 0.75 and 0.85. For this project, the data are already treated, so only the power spectral densities, the correlations between couples of sensors and RMS of Kulites are available. The model is equipped with 62 Kulites (all in the outboard part of the wing). Figure 4d shows their locations on the suction side of the wing. The acquisition of dynamic data is performed at 2048 Hz with a low-pass filter at 750 Hz.

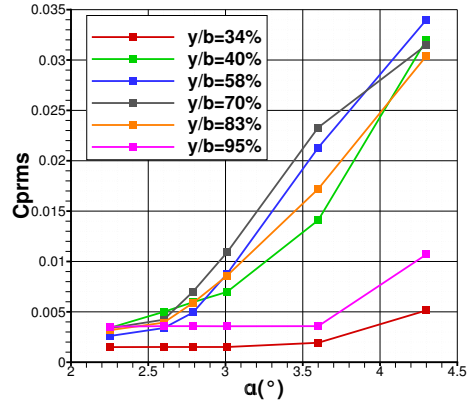
III. Buffet onset

Definition of the range where the buffet phenomenon appears is the first step in the analysis of experimental results, so value of the buffet onset and possibly buffet exit are given in the following.

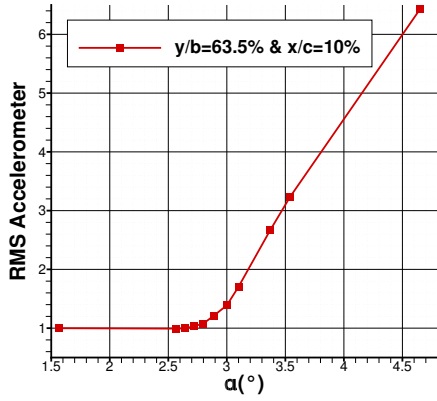
Determination of the buffet exit is more complicated. Contrary to the 2D buffet case, an exit in the 3D case has never been observed. It is one other difference with the 2D transonic buffet where it was shown that the shock wave on the airfoil becomes unstable and subsequently stabilizes again at higher values of angle of attack and/or Mach number (see ref. [8]). While for the onset different criteria are presented in the following. The main difference is between local and global criteria. It is possible to consider global criteria as criteria based on the structural response of the wing or based on integral variables like for example the analysis of the lift curve or the RMS value of the accelerometers. Concerning the lift curve, the buffet onset angle of attack is defined by the intersection between the lift curve and a straight line parallel to the linear part of the lift curve shifted by $+0.1^\circ$. Concerning the analysis of accelerometers, the buffet onset is defined in the present paper when the RMS value exceeds 1.4 times the rest value. The local buffet criteria are based on the analysis of the mean pressure value at the trailing edge or the RMS of the unsteady pressure transducers.



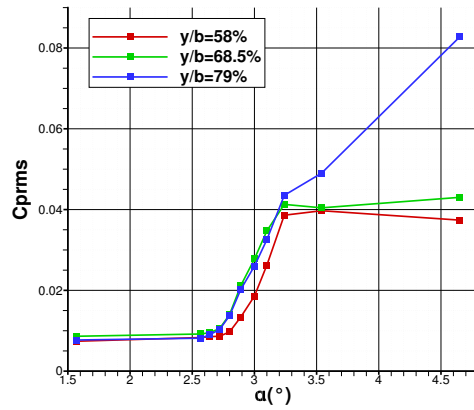
(a) RMS of Kulites for BUFET'N Co close to TE at $M=0.82$.



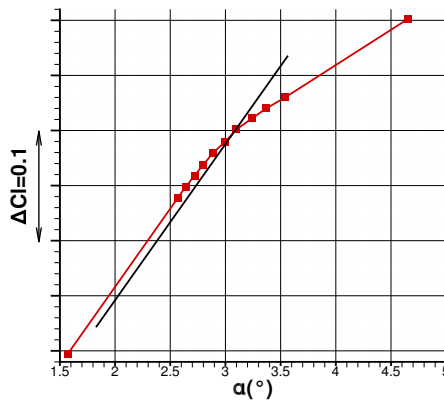
(b) RMS of Kulites for DTP Tremblement close to TE at $M=0.8$.



(c) RMS of accelerometer close to the wing tip for FLIRET project at $M=0.85$.



(d) RMS of Kulites for FLIRET close to TE at $M=0.85$.



(e) Lift curve for FLIRET project at $M=0.85$

Fig. 5: Buffet onset criteria.

These criteria have to be applied on each section of the wing to help find in which section buffet appears first. The onset is defined when the static value of C_p at the trailing edge diverges more than 0.05 or when the RMS value exceeds 2.5 times the initial plateau (far before buffet onset, the RMS of Kulites are constant as shown in figure 5d).

Figure 5 shows the application of different criteria for three of the four test cases. AVERT, for which buffet onset is found at about 3° , is not shown here because it is already available in figure 5 of Dandois [14]. Here four different criteria are analyzed, two globals and two locals: the RMS of the accelerometers at wing tip, the kink on the lift curve, the RMS of the Kulites and the value of static pressure at the trailing edge. For each test case, the different criteria agree well with each other.

The buffet onset is very clear for the FLIRET test at $\alpha \cong 3^\circ$ for which the RMS of the Kulite signal at $y/b = 79\%$ and the RMS of the accelerometer start to diverge. Concerning the DTP Tremblement case, only the RMS of the Kulites are available and the onset is found at $\alpha \cong 3.1^\circ$. For the BUFFET'N Co case, buffet onset is found at $\alpha \cong 3^\circ$ from the RMS of the Kulites.

Finally it is very interesting to define buffet onset in the M - α plane. Figure 6 shows the α onset

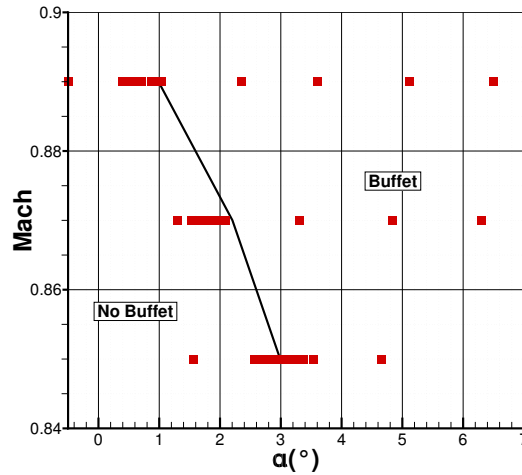


Fig. 6: Buffet onset line in the M - α plane for FLIRET project

for the FLIRET case at different values of the Mach number. The higher the Mach number, the lower the angle of attack for which buffet onset occurs.

IV. Power Spectral Densities

The analysis of the power spectral densities is probably the parameter that most defines the phenomenon. As already said the main difference between 2D and 3D buffet is the increase of shock frequency oscillation. The PSDs are analyzed on the whole wing, i.e. in the chordwise and spanwise directions, in order to get the spatial variations of the buffet frequency.

The PSDs do not reveal only the transonic buffet frequency. Indeed, depending on the frequency sampling of each test, it can also exhibit other physical phenomena. For example, the Kelvin-Helmholtz (KH) instability, which renders shear-layers with inflection points unstable, appears in the frequency range [1000-4000 Hz]. The theoretical frequency is around $f_{KH} = 0.135U/\delta_\omega$, where U is the average velocity above and below the shear layer and δ_ω the vorticity thickness (see [25] for more details). The KH instability should appear in every spectra but AVERT, FLIRET and DTP Tremblement overlook the phenomenon due to a low pass filter applied to each signal. Nevertheless it is still possible to observe the KH instability in the frequency-wavenumber spectra for AVERT and FLIRET projects. This is because the frequency-wavenumber ($k-f$) spectrum is based on the coherency of the signals, so even if signals are filtered the high coherency zones remains. The only campaign that shows the KH instability in both PSD and cross-spectrum is the BUFFET'N Co one for which the sampling frequency is much higher, 20480 Hz.

In order to compare the results over different models a non dimensional number is defined for the buffet frequency, the Strouhal number $St = (fL)/U_\infty$ where f is the frequency, L the characteristic length and U_∞ the freestream velocity. There are different choices for the characteristic length L : the local chord and two kinds of mean aerodynamic chord (classical MAC and a MAC defined only on the external part of a double swept wing labelled MAC' for FLIRET and DTP Tremblement wings). Consequently, different Strouhal numbers can be defined. The reason lies in the different point of views on the phenomenon, local or global in space: local Strouhal number means an analysis only at a given section, so with the value of the chord at this section. While the Strouhal number based on the MAC tries to define a global value for the entire wing, like if there was an unstable

global mode which synchronizes all sections. Furthermore, for wings with a high value of the taper ratio, it is compulsory to consider the local Strouhal number in order to perform comparisons with small taper ratios (like FLIRET and BUFET'N Co tests).

A. PSDs for the BUFET'N Co case

BUFET'N Co tests are performed at Mach number 0.82 and α ranges from 2.5° to 3.5° . The Kelvin-Helmholtz instability clearly appears in the spectra at its typical frequency (1000-4000 Hz) when approaching the TE, because the flow is more separated. The intensity of the instability increases approaching the wing tip, except for the final flow reattachment due to the wing tip vortex. Figure 7 clearly shows two different bumps: one for buffet and one for KH instability.

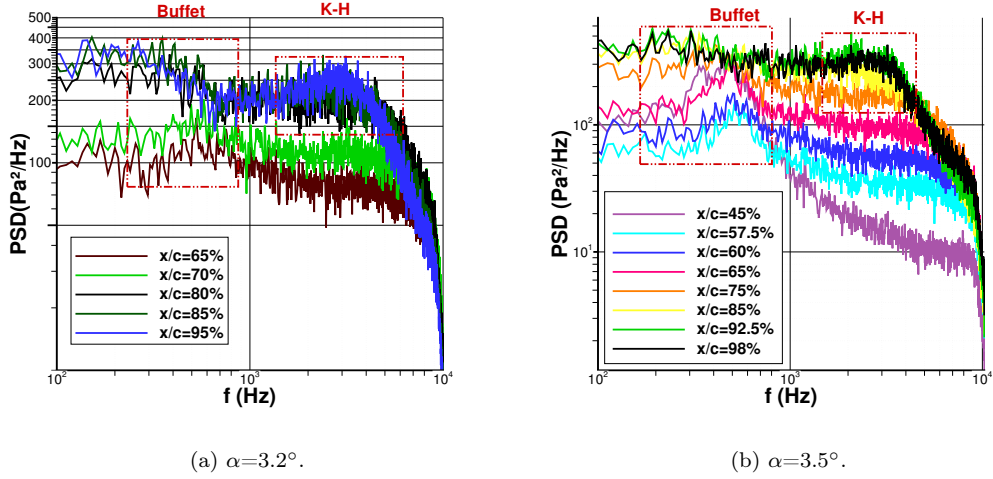


Fig. 7: Log-log graph of power spectral densities for BUFET'N Co test at $M=0.82$ in the chordwise direction at $y/b=60\%$.

The buffet onset is found at $\alpha \cong 3^\circ$. Close to the onset at $\alpha = 3.2^\circ$, the bump in the spectra is very large and centered about 430 Hz ($St_{MAC} = 0.34$). Here the variations of the frequency in span and chord are very weak (figure 7a; it is even difficult to visualize buffet peak approaching the TE).

At $\alpha \cong 3.5^\circ$, so in well-established transonic buffet, the situation is relatively different. It

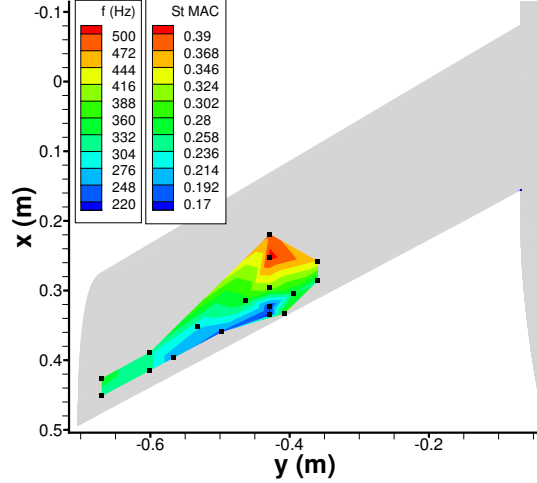
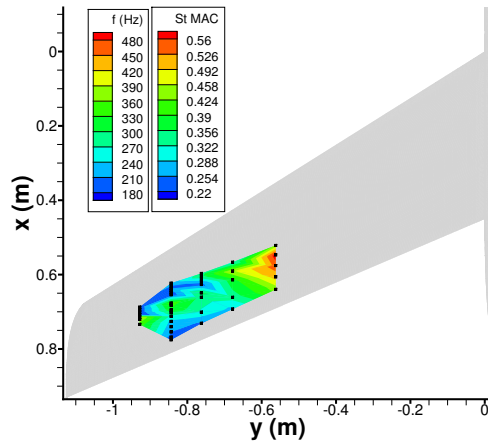


Fig. 8: Buffet frequency map for BUFET'N Co test at $\alpha=3.5^\circ$ and $M=0.82$.

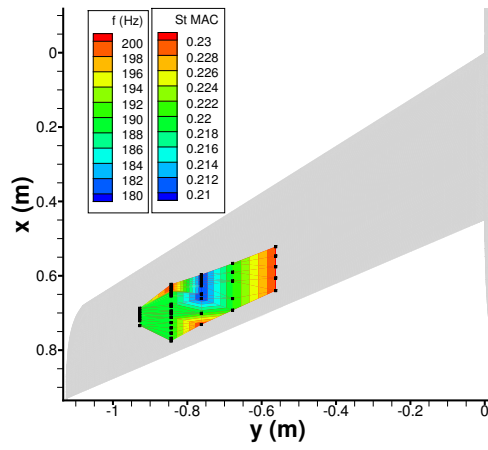
is easier to identify the bump in the spectra and the variations in the chordwise and spanwise directions are clearer. The analysis is focused on the section at $y/b = 60\%$ (figure 7b), the section that first enters into buffeting and which is best equipped with sensors. In the chordwise direction, as already mentioned by Dandois [14], the buffet frequency decreases from around 430 Hz ($St_{MAC} = 0.34$) at 60% of the chord to 250 Hz ($St_{MAC} = 0.2$) at the TE. A spanwise variation of the buffet frequency is observed with an oscillation between the critical section and the wing tip: the buffet frequency decreases up to $y/b = 60\%$ (where the KH instability is the strongest), then increases before a final decrease at the wing tip. The map in figure 8 shows the variations of buffet frequency on the wing.

B. PSDs for the AVERT case

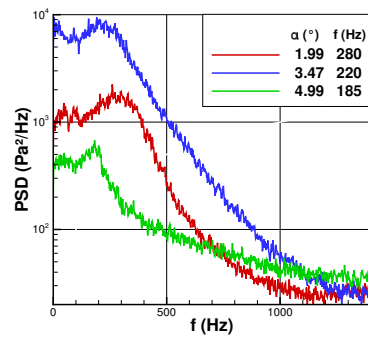
In the AVERT project several values of α were tested at Mach numbers: 0.78, 0.8, 0.82, 0.84 and 0.86. The analysis is focused on the tests performed at $M = 0.82$. AVERT project has already been analyzed by Dandois [14], so here the results are presented in comparison with the other databases.



(a) Buffet frequency map at $\alpha=3.47^\circ$ and $M=0.82$.



(b) Buffet frequency map at $\alpha=4.99^\circ$ and $M=0.86$.



(c) Semi-log graph of power spectral densities at shock foot and $y/b=75\%$ for $M=0.86$ with values of buffet frequencies in the legend.

Fig. 9: PSDs for the AVERT project.

Typical values of buffet frequency around 210-220 Hz ($St_{MAC} = 0.25-0.27$) are identified on the PSDs. At $\alpha \cong 3.5^\circ$, so in well-established buffet conditions (figure 9a), the frequencies vary a lot on the wing, so points at $y/b = 75\%$ and towards the TE are considered as reference for the definition of the typical frequency range. Besides, as noted for the onset in BUFET'N CO, the buffet frequency variations on the wing are smaller at higher incidence (figure 9b). Figure 9a shows the map with values of buffet frequency over the wing at $M = 0.82$ and $\alpha = 3.47^\circ$ showing physical frequency in Hertz and Strouhal number based on MAC . It shows how the buffet frequency varies on the wing, precisely it decreases in the chord and span directions.

Figure 9c shows the reduction of buffet frequency with α at $M = 0.8$. It shows PSDs at shock foot for $\alpha = 1.99^\circ$ and $\alpha = 3.47^\circ$ while for $\alpha = 4.99^\circ$ the most upstream sensor at $x/c = 40\%$ is not exactly at the shock foot, this is the reason why the PSD level is low (but for this case the peak does not move in chord so the conclusion is the same).

C. PSDs for the FLIRET case

Five values of the Mach number are considered: 0.85, 0.87, 0.89, 0.91 and 0.93; while the angle of attack is not piloted uniformly. The angles of attack are chosen in order to be centered around buffet onset. There is no transition triggering thanks to a cryogenic temperature of 162K that gives a sufficiently high Reynolds number (using MAC as reference length: 8.2×10^6 to 70.5×10^6).

FLIRET is the project with the larger range of Mach numbers and α . Consequently a large buffet frequency range is found analyzing all the PSDs of the tests. It is possible to find values from 220 to 600 Hz ($St_{MAC} = 0.22-0.95$). The lowest values of buffet frequency are usually found around the wing tip in the well-established buffet regime (i.e. for high values of α). At the onset ($\alpha = 3^\circ$), the buffet frequency is roughly constant all over the wing around 420-500 Hz ($St_{MAC} = 0.65-0.8$). More precisely, buffet is not present on the entire wing but only in the most critical section at about 75-80% of span. At higher values of α , the areas in buffet

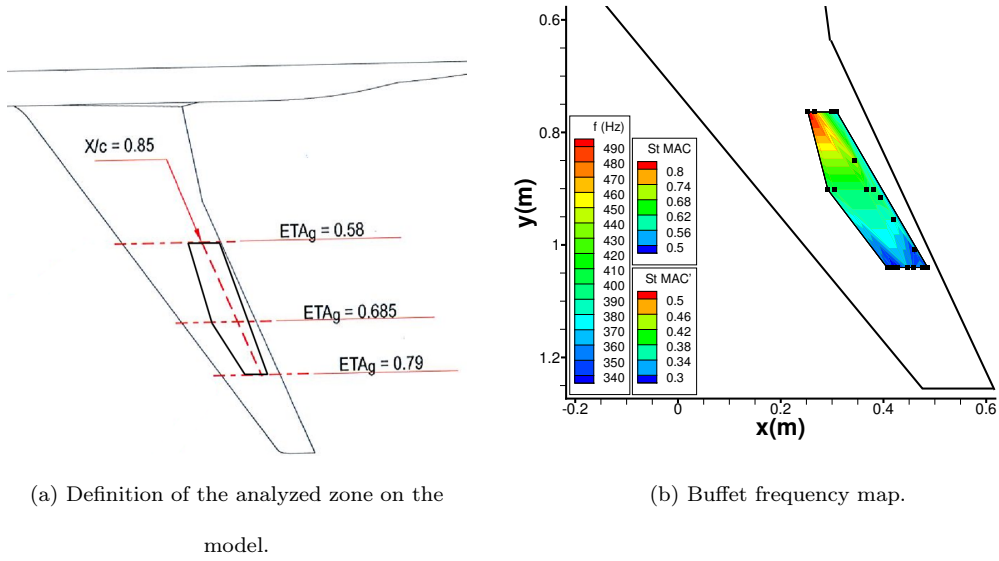


Fig. 10: Buffet frequency map for FLIRET case at $\alpha=3.37^\circ$ and $M=0.85$

conditions, which correspond to the separated zones, increase; the value of the buffet frequency decreases and variations of frequency start to appear: it decreases towards the wing tip and a little bit in chord as well (figure 10). The variations in chord are less clear than in span, especially towards the wing tip (figure 11). However the same variations of buffet frequency in the wing direction (chord and span) and with α than in BUFET'N Co and AVERT cases are found here.

It is compulsory in a comparison between models with such different geometries to identify characteristics lengths that better fit the non-dimensional numbers. Here because of the high taper ratio of the model, the Strouhal number based on the local chord length is used. In this case the Strouhal range of figure 10 is reduced to 0.2-0.35 with a characteristic value of 0.25 in $x/c = 85\%$ and $y/b = 79\%$. A comparison between the Strouhal based on the local chord and the two kinds of mean aerodynamic chord shows that the range of Strouhal decreases from 0.5-0.8 (based on MAC) to 0.3-0.5 (based on MAC') and finally 0.2-0.35 (based on local chord).

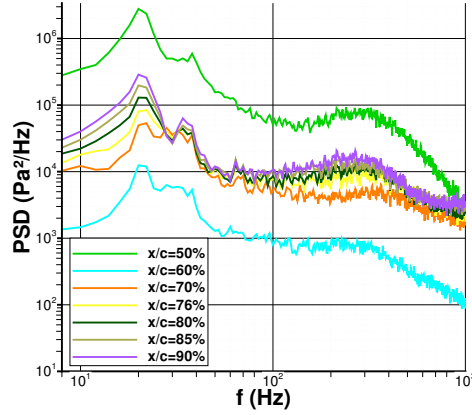


Fig. 11: Log-log graph of power spectral densities for FLIRET at $\alpha=3.61^\circ$ and $M=0.85$ in the chordwise direction at $y/b=79\%$.

D. PSDs for the DTP Tremblement case

For this database, only root mean square values of the sensors signal, cross-spectra (coherency and phase) and PSDs are available. The resolution of these treatments in the frequency domain is 25 Hz and the frequency range of analysis is 0-750 Hz, both too low for the visualisation of the KH instability. There are Mach numbers of 0.75, 0.8, 0.825 and 0.85 for various α . In particular are analyzed a series of tests at Mach number 0.8, with nacelle, stabilizers and boundary layer transition fixed at 10%.

Here, as in FLIRET project, a large range of buffet frequency is found. The reasons are twofold. First the range of M - α analyzed is very large. While the second reason is identified inside the geometry of the double swept wing. Buffet frequency from 225 to 400 Hz are found ($St_{MAC} = 0.18$ to 0.36). All the other peaks are the structural modes (like the peaks at 125 Hz in figure 12). It is interesting to highlight the difference between buffet onset and well-established buffet conditions. For the first case the buffet frequency is rather constant on the wing and even hard to be identified on the PSDs. While at higher α the outlook of the PSDs are clearer: a value of 300 Hz ($St = 0.19$ based on local chord, 0.28 based on MAC and 0.22 based on MAC') is found at $M = 0.8$ and $\alpha = 3.6^\circ$ at $y/b = 70\%$ (here considered as the critical section) while a smaller value of 225 Hz

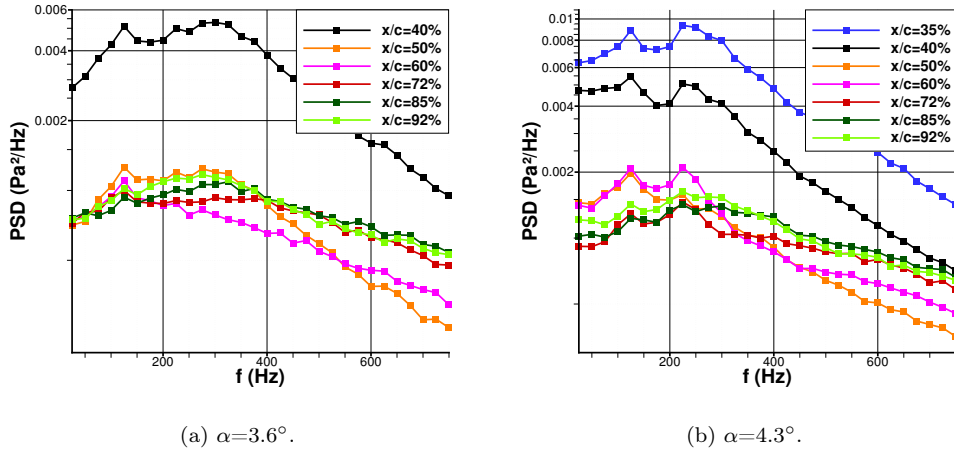


Fig. 12: Semi-log graph of power spectral densities for DTP Tremblement at $M=0.8$ in the chordwise direction at $y/b=70\%$.

($St = 0.14$ based on local chord, 0.21 based on MAC and 0.16 based on MAC') is found on the same section at $\alpha = 4.3^\circ$ (figure 12). The figures show that the buffet frequency decreases and is more a peak than a bump when increasing α at a fixed Mach number.

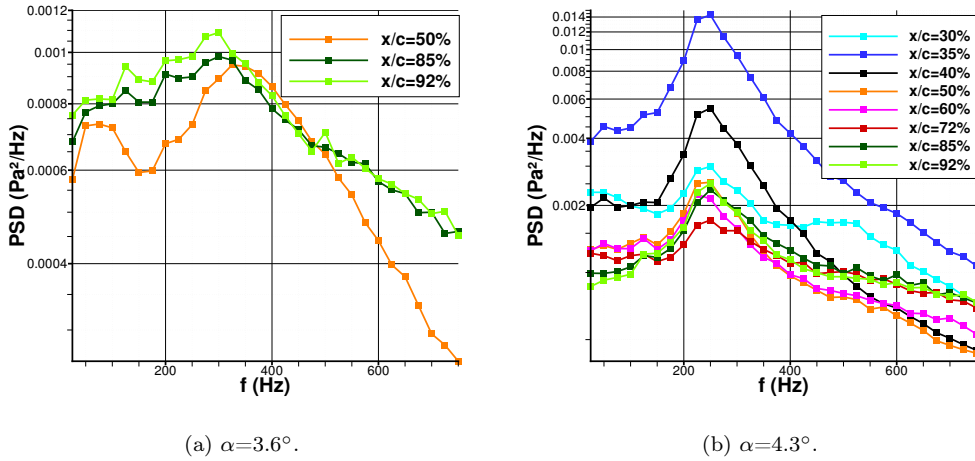


Fig. 13: Semi-log graph of power spectral densities for DTP Tremblement at $M=0.8$ in the chordwise direction at $y/b=58\%$.

Other tests are analyzed in order to get the variations of buffet frequency on the wing. There is a clear decrease in chordwise directions at $\alpha = 3.6^\circ$ (figure 13a) while buffet frequency remains

more constant at higher α (figure 13b). In the same way, a comparison between figure 13a and figure 12a shows a decrease of the frequency buffet in the spanwise direction, from 300-350 Hz to 275-300 Hz.

Finally, in the DTP tremblement project, it is found out that buffet is the only physical phenomenon that appears on the spectra because of the low frequency sampling.

V. Cross-Spectral analysis

Signal processing tools such as cross-spectra or frequency-wavenumber spectra are shown in the following. They are an efficient way to determine the convection velocities of the 3D buffet phenomenon (and of the KH instability). These velocities are defined for a fixed value of frequency, or at least a range, in order to strictly link the velocity to the physical phenomenon appearing at the considered frequencies.

A. Cross-Spectrum

Cross-spectrum is the Fourier transform of the cross-correlation of two stochastic processes, in the present case the measured signals from the Kulites. If $x_1(t)$ and $x_2(t)$ are two continuous signals, the cross-correlation $R_{x_1x_2}(\tau)$ is the convolution of the signals.

$$R_{x_1x_2}(\tau) = \int_{-\infty}^{\infty} x_1(t)x_2(t + \tau)dt \quad (1)$$

The Fourier transform \mathcal{F} switches the cross-correlation $R_{x_1x_2}(\tau)$ from time to frequency domain defining in this way the cross-spectrum $\hat{R}_{x_1x_2}(f)$. An interesting properties in the Fourier space is that the convolution of two signals in time is just the product of the Fourier transform of the two signals.

$$\hat{R}_{x_1x_2}(f) = \mathcal{F}\{R_{x_1x_2}(\tau)\} = \int_{-\infty}^{\infty} R_{x_1x_2}(\tau)e^{-2\pi i\tau f}d\tau \quad (2)$$

$$\hat{R}_{x_1x_2}(f) = \mathcal{F}\{R_{x_1x_1}(\tau)\} * \mathcal{F}\{R_{x_2x_2}(\tau)\} \quad (3)$$

The cross-spectrum $\hat{R}_{x_1x_2}(f)$ in polar coordinates shows the amplitude $\hat{A}_{x_1x_2}(f)$ and the phase $\Phi_{x_1x_2}(f)$ of the function. The phase is the main parameter in order to defined the convection velocity while the square of the amplitude divided by the spectra of the two signals gives the coherency γ^2 .

$$\hat{R}_{x_1x_2}(f) = \hat{A}_{x_1x_2}(f)e^{i\Phi_{x_1x_2}(f)} \quad (4)$$

$$\gamma_{x_1x_2}^2(f) = \frac{\hat{A}_{x_1x_2}^2(f)}{\hat{R}_{x_1x_1}(f) * \hat{R}_{x_2x_2}(f)} \quad (5)$$

The coherency allows to identify the range in the frequency domain where there are convective phenomena, and from the phase difference, it is possible to compute the velocities. Normally there are high values of the coherency at the buffet frequency; then there are two ways to estimate the convective velocities. The two methods are based on the same idea and give almost the same results. One is to choose a single value of frequency for which the coherency is high and look at linear variations of phase difference in the space domain. It is very precise in terms of frequency while it is averaged in the space domain considered. Convection velocity is obtained using the relation $U_C = 2\pi f \Delta x / \Delta \varphi$ where f is the selected frequency in Hertz, Δx the distance between the sensors in meters and $\Delta \varphi$ the phase difference in radians. The second method is computed between two sensors and the results of coherency and phase are analyzed in the frequency domain. The range of frequency with high coherency shows linear variation of phase difference. From this slope, it is possible to obtain the convection velocity, $U_C = 2\pi \Delta x \Delta f / \Delta \varphi$ where the variables are the same as above except for Δf which is here a range and not a single value. This case is more precise in space because just two sensors are analyzed but averaged in the range of frequency looked, this is the reason why it is important to consider only the frequency range of the interesting phenomenon. Figure 14 shows an example of the analysis of a cross-spectrum for two sensors of the BUFET'N Co test. It is possible to see that the coherency is high only in the buffet frequency range so a linear slope is found in the phase plot.

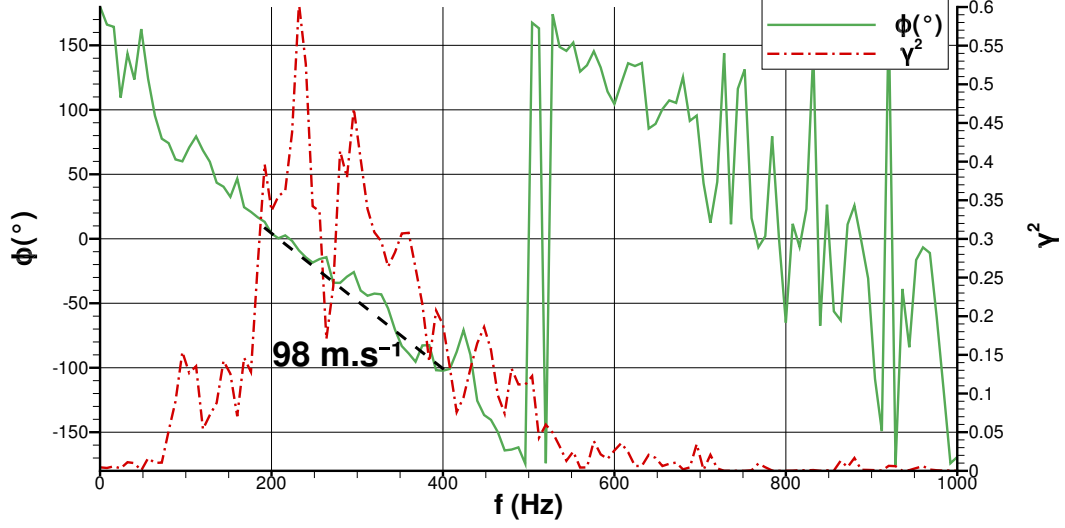


Fig. 14: Cross-spectrum coherency and phase at $x/c=80\%$ on the suction side of the wing between two sensors at $y/b=75\%$ and 95% for $\alpha=3.5^\circ$ and $M=0.82$ for BUFET'N Co test. Black dotted line is the slope considered in the buffet frequency range 200-400 Hz (defined thanks to buffet frequency map in figure 8) in order to calculate the convection velocity.

Once defined the velocity both in the spanwise and chord wise directions it is possible to compute the full velocity vector, so its norm and direction. The chordwise and spanwise velocities are not combined in the classical vectoral way but following Larchevêque [26]:

$$\begin{cases} U_C &= U_{C_c} \cos \beta \\ U_C &= U_{C_s} \sin(\beta - \Lambda) \end{cases} \quad (6)$$

with β the angle between the wave propagation direction and the chordwise one (shown in figure 15). U_{C_c} and U_{C_s} are the convection velocities in the chordwise and spanwise directions respectively found by the cross-spectrum analysis. Λ is the wing sweep at the considered point and U_C is the wave convection velocity norm.

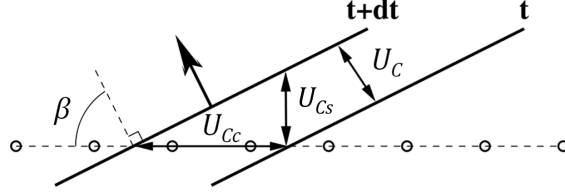


Fig. 15: Impact of the wave direction on the measured velocity U_{Cc} , on a line of sensors [26].

B. Frequency-wavenumber spectra

The analysis of the frequency-wavenumber spectra is another way to compute the convection velocity. It is based on an estimator $\psi(f, k)$ which depends on the cross-spectral matrix $\Psi(f)$. Since in space the definition of a transform is not possible because the sensors are not equidistant, an estimator is defined (see [26] for more details):

$$\psi(f, k) = \eta^H(k) \Psi(f) \eta(k) \quad (7)$$

Where H is the Hermitian transpose, k is the wavenumber and $\eta(k)$ and $\Psi(f)$ are defined by:

$$\begin{cases} (\Psi(f))_{ij} &= \hat{R}_{x_i x_j}(f) \\ (\eta(k))_i &= e^{-ikx_i} \end{cases} \quad (8)$$

The obtained spectrum is function of frequency and wavenumber, so it is possible to distinguish several phenomena by looking at different frequency ranges and then to compute for each phenomenon the corresponding convection velocity. Phase velocities ($U_p = 2\pi f/k$) are found with the cross-spectra, while in the $k - f$ spectra it is possible to find both phase and group velocities. The group velocity is the propagation of the real information of the waves, the envelope of a signal. It is defined as the variation of the angular frequency δf with the wavenumber, $U_g = 2\pi \delta f / \delta k$. The two velocities found are similar, precisely the difference is smaller than the error incertitude. So it is possible to state that the phenomenon is not much dispersive.

In the following the results of $k - f$ spectra are presented. In all the figures the frequency is in Hertz while the wavenumber is non-dimensionalized by chord or span. Figure 16 shows the results

for one selected case of BUFET’N Co test and it is in complete agreement with Dandois [14]. It is possible to identify the Kelvin-Helmholtz instability in the frequency range [1000-4000Hz] as well as the buffet phenomenon in the frequency range [200-500Hz]. The magnitude of the velocities comes from the slope in the $k - f$ spectrum $U_C = 2\pi \Delta f / \Delta k$. At this moment, it is important to look at two different spectra, in chord and in span. The velocities in the spectra are used together with equation (6) to define the velocity norm and the propagation direction of the phenomenon. In this case, the Kelvin-Helmholtz propagates mostly in the chordwise direction (indeed it does not appear in the spanwise direction); the resulting velocity is typical of this instability 180 m.s^{-1} or $0.65U_\infty$ (see [14], [27] and [28]). While for the buffet velocity the spectra in chord at $y/b = 60\%$ gives 90 m.s^{-1} , the $k - f$ spectrum in span at $x/c = 80\%$ gives 70 m.s^{-1} so from eq. (6), this results in a buffet velocity norm of 66 m.s^{-1} , or a non-dimensional convection velocity of $0.24U_\infty$ with an angle of $\beta = 43^\circ$.

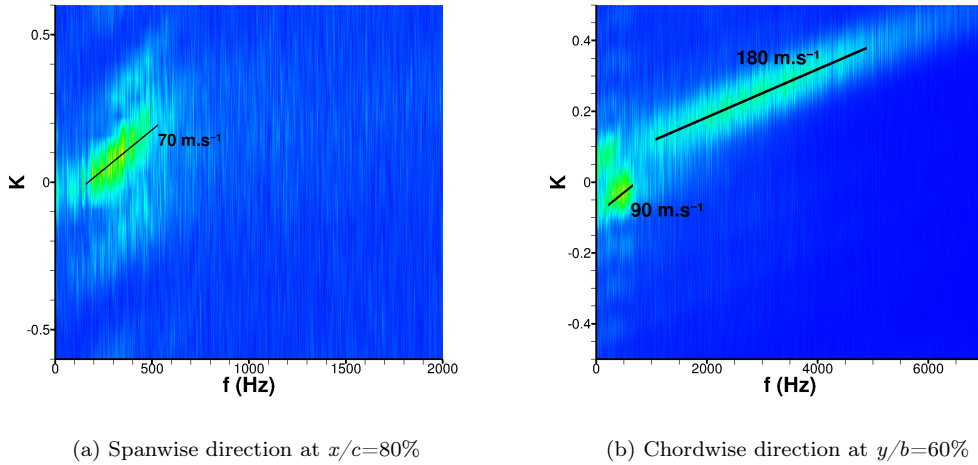


Fig. 16: Frequency wavenumber spectrum for BUFET’N Co project at $\alpha=3.5^\circ$ and $M=0.82$.

The spectra of BUFET’N Co test for other values of M or α show no convection velocities before buffet onset and the same results as in figure 16 for the case in buffet. The range of M - α tested is smaller than for the other tests so it impossible to look at the complete evolution of these velocities. This is not the case for FLIRET and AVERT projects where the M - α range is larger.

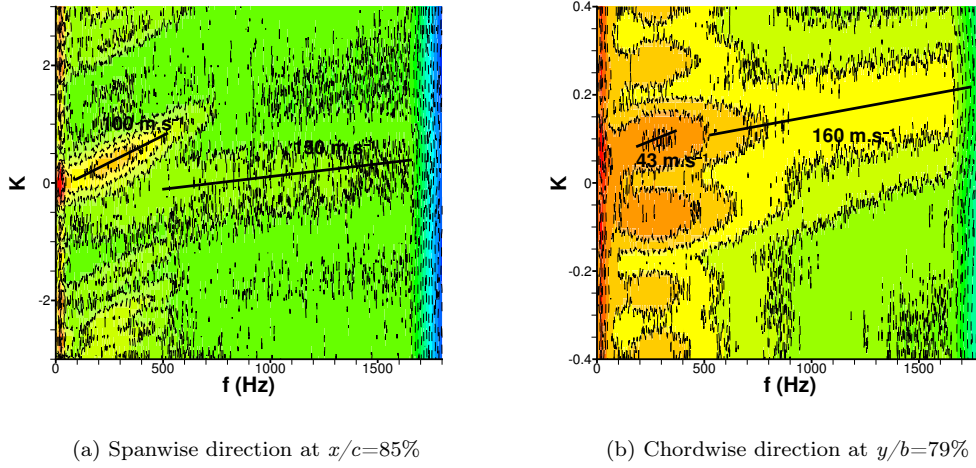


Fig. 17: Frequency wavenumber spectrum for FLIRET project at $\alpha=3.37^\circ$ and $M=0.85$.

The results are a little different for the FLIRET tests. The reference test at $M = 0.85$ and $\alpha = 3.37^\circ$ (figure 17) gives both buffet and KH velocities at $y/b = 79\%$ and in chord at $x/c = 85\%$ while just buffet velocity appears clearly at $y/b = 58\%$ and 68.5% . Combining the couple of velocities in chord and span, the results are a non-dimensional convection velocity of $0.24U_\infty$ with an angle of 2° for the buffet and $0.63U_\infty$ with an angle of 52° for KH instability (the wind tunnel is cryogenic, so the velocities are lower and just the non-dimensional velocities are considered here).

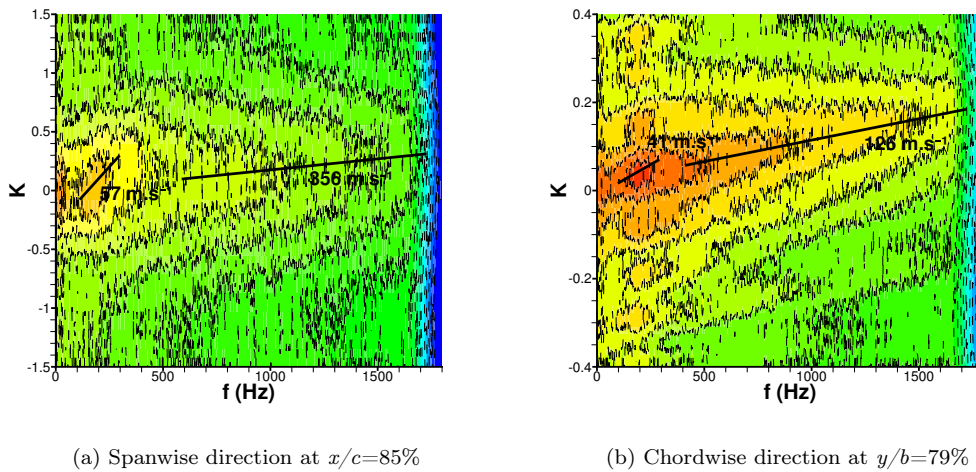
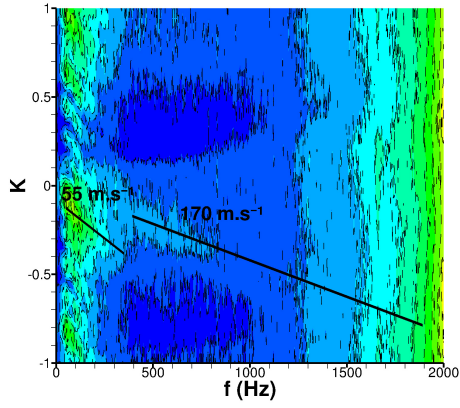


Fig. 18: Frequency wavenumber spectrum for FLIRET project at $\alpha=4.84^\circ$ and $M=0.87$.

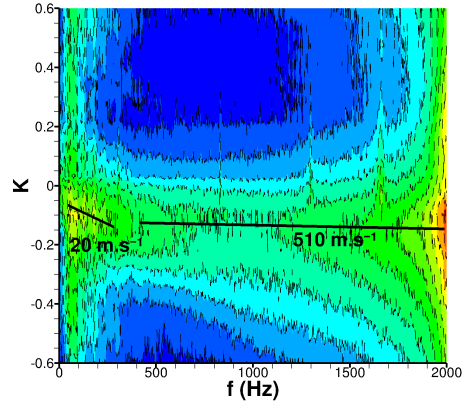
For a higher Mach number of 0.87 and $\alpha = 4.84^\circ$, figure 18 shows an example of the $k - f$ spectra at $x/c = 85\%$ and $y/b = 79\%$. Combining the velocities in chord and span the results are a non-dimensional convection velocity for buffet of $0.2U_\infty$ with an angle of 19° and for KH instability of $0.61U_\infty$ with an angle of 4° . The KH instability is more oriented towards the chordwise direction. While buffet convection velocity is more oriented in spanwise direction and it is also slightly smaller than the typical value of $0.24U_\infty$; both are considered as effects of higher α .

The $k - f$ spectra analysis for the AVERT test adds some interesting phenomena in comparison with the other projects and with the previous work of Dandois [14]. Above all, it is very interesting to look at the precise evolution of the convection velocity for different angles of attack. Figure 19 shows the $k - f$ spectra in chord and span (at x/c and y/b both 75%) for all the tests at Mach number 0.86, they represent the α evolution of the test: 0° , 1.99° and 3.47° . For this value of the Mach number, the buffet onset is at $\alpha = 1^\circ$ (see figure 6 of Dandois [14]).

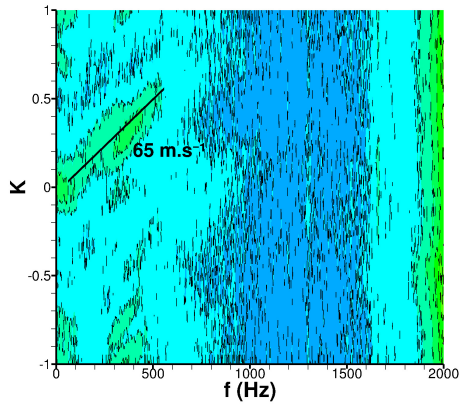
In the following, only the final value and direction of the convection velocities are given, so after the correction of the angle and the combination of the chordwise and spanwise components following equation (6). The analysis starts at $\alpha = 0^\circ$ (figure 19a and 19b), where it is possible to see two upstream convection velocities both in chord and span. The first is in the low frequency range, precisely [0-100 Hz]. It is a convection velocity at about 20 m.s^{-1} ($0.07U_\infty$) with an angle of 194° , it is the propagation of a low frequency acoustic wave, and indeed it is exactly equal to $U_{(x,wing)} - a$, where $U_{(x,wing)}$ is the chordwise velocity downstream of the shock and a the speed of sound. The second velocity acts on a larger range of frequency [200-2000Hz] and it has a magnitude of about 180 m.s^{-1} ($0.64U_\infty$) with an angle of 250° . It is also an acoustic wave, indeed the same magnitude is found performing $U_{(s,wing)} - a$, where $U_{(s,wing)}$ is the velocity in the spanwise direction on the wing and a the speed of sound. The two upstream acoustic waves are generated respectively at the TE and the wing tip. Increasing α to 2° (figure 19c and 19d) there is a crucial point. In the chordwise $k - f$ spectrum there are four different convection velocities: the two upstream already described (with the same values of magnitude and direction) and two other downstream



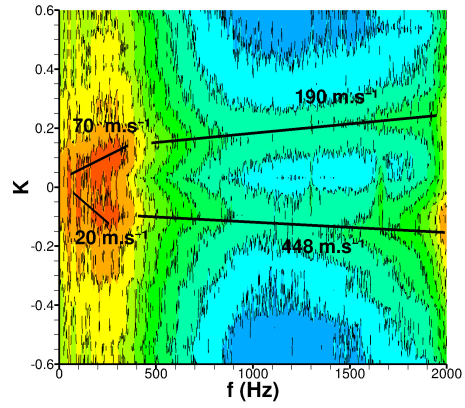
(a) Spanwise direction at $x/c=75\%$ and $\alpha=0^\circ$



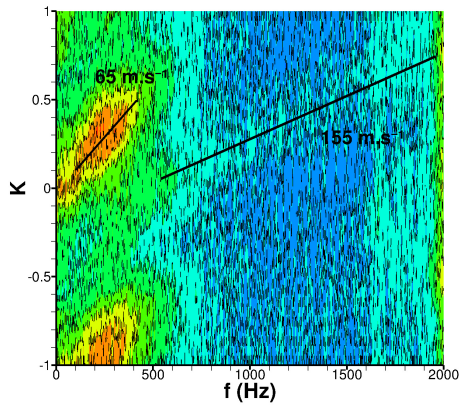
(b) Chordwise direction at $y/b=75\%$ and $\alpha=0^\circ$



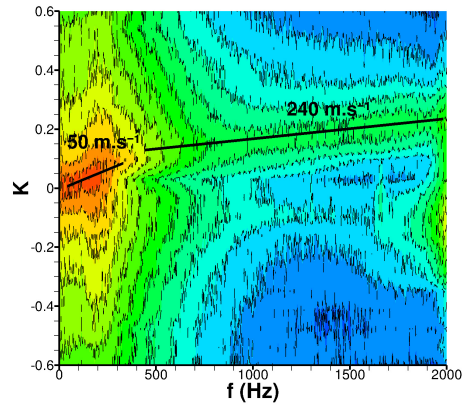
(c) Spanwise direction at $x/c=75\%$ and $\alpha=1.99^\circ$



(d) Chordwise direction at $y/b=75\%$ and $\alpha=1.99^\circ$



(e) Spanwise direction at $x/c=75\%$ and $\alpha=3.47^\circ$



(f) Chordwise direction at $y/b=75\%$ and $\alpha=3.47^\circ$

Fig. 19: Frequency wavenumber spectrum for AVERT project at $M=0.86$.

convection velocities, one at low frequency [50-400Hz] and the other one all along the frequency range of the spectrum [400-2000Hz]. The low frequency convection velocity has a magnitude of 57 m.s^{-1} ($0.21U_\infty$) and an angle of 36° ; these values of direction, magnitude and frequency range are consistent with a buffet convection velocity. The other downstream convection velocity appears only in chord with a magnitude of 190 m.s^{-1} ($0.65U_\infty$). The value of magnitude and the frequency range are consistent with a Kelvin-Helmholtz convection velocity and as in BUFET'N Co project it propagates in the chordwise direction. When α reaches the values of 3.47° (figure 19e and 19f), the upstream velocities disappear and just the two downstream ones remain. It is still possible to see the upstream high frequency acoustic velocity very weak (figure 19f) because they do not really disappear, they are just covered by other phenomena. The buffet convection velocity decreases: 48 m.s^{-1} ($0.17U_\infty$) with an angle of 20° . While the KH convection velocity has a magnitude of 175 m.s^{-1} ($0.63U_\infty$) but now it appears in span as well with a $\beta = 51^\circ$, very close to the values and direction found for FLIRET in figure 17. Finally at $\alpha = 5^\circ$ (figures not showed) buffet velocity is at 47 m.s^{-1} ($0.17U_\infty$) with $\beta = 30^\circ$ and KH velocity is at 170 m.s^{-1} ($0.6U_\infty$) with a reduction of $\beta = 15^\circ$.

C. Convection velocity

Finally it is possible to defined the values of the convection velocities. They are computed over the entire wing in some characteristics points. As already said the results of cross-spectra and $k - f$ spectra are consistent with each other.

For each wind tunnel test, the cases considered are the most similar ones in terms of $M-\alpha$. For both BUFFET'N Co and AVERT, α is equal to 3.5° and the Mach number is equal to 0.82. For FLIRET, the Mach number is 0.85 and $\alpha = 3.37^\circ$ and for DTP Tremblement, the Mach number is 0.8 and $\alpha = 4.2^\circ$. Figure 20 shows the physical velocity expressed in m.s^{-1} for these cases. For the AVERT case, the figure is taken from Dandois [14] with the correction of the right angle in equation (6).

All models exhibit convective velocities both in the chordwise and spanwise directions. The

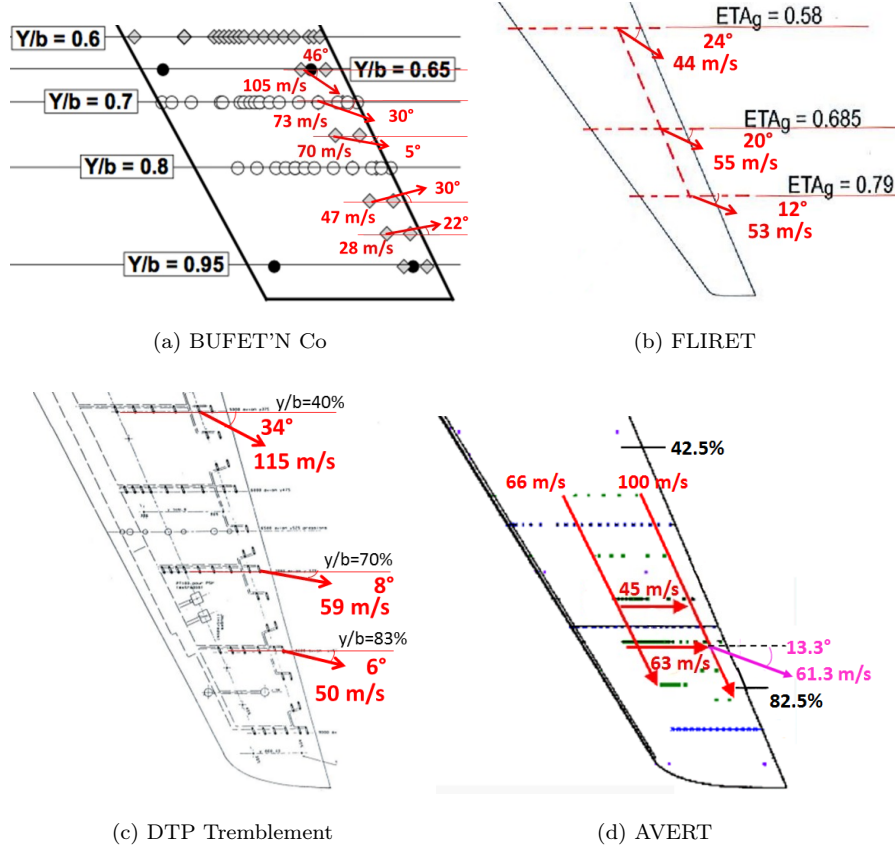


Fig. 20: Convection velocity on the external part of the wing for the four wind tunnel tests. The cases analyzed are given in table 1.

second one is characteristic of the 3D transonic buffet because it is probably the main cause of the “buffet cells” convection as identified by Iovnovich & Raveh [22]. FLIRET and BUFET'N Co show similar values of the convective velocities close to the trailing edge, about $0.26U_\infty$, while DTP Tremblement and AVERT have slightly lower values ($0.235 \pm 0.005 U_\infty$). By the way the resulting non-dimensional convective velocities are consistent with each other. Directions are not always the same because linked with the shape of the wing while for the magnitudes the consistency is better.

VI. Synthesis and physical discussions

The present work consists in the comparison of experimental results for the four different databases. The models are different in terms of chord length, taper ratio, twist and geometry in general but they are all based on supercritical airfoils. Power spectral densities, cross-

spectra and frequency-wavenumber spectra of the unsteady pressure measurements have been analyzed as well as static pressure and accelerometers. The main results of the experimental analysis are summarized in Table 1. It is noteworthy that they are essentially consistent with each other.

A. Summary

Table 1: Summary of the main results for the four databases analyzed. In the first line there are projects names and the points where precise Strouhal and convection Mach are evaluated.

Projects:	AVERT	BUFET'N Co	FLIRET	DTP Trembl.
	x/c 87.5% y/b 75%	x/c 80% y/b 70%	x/c 85% y/b 79%	x/c 80% y/b 70%
Onset	$\approx 3^\circ$	$\approx 3^\circ$	$\approx 3^\circ$	$\approx 3.1^\circ$
St (local c)	0.22	0.24	0.27	0.26
St (MAC)	0.26	0.27	0.48	0.3
St (MAC')			0.33	0.23
U_C/U_∞	0.24	0.26	0.26	0.23

It has been shown that 3D buffet appears with high frequency values in comparison to 2D, especially for the well-established or deep buffet regime. While at the onset peaks of PSDs are not so clear and the clear ones are more linked to 2D than 3D buffet. Low frequency peaks are found in some cases as in AVERT at $\alpha = 3^\circ$ and $M = 0.82$ (see figure 13 of Dandois [14]). Figure 21 shows the resulting phase from cross-spectra at five selected frequencies (the only ones with high coherency): the buffet phenomenon is more 2D than 3D, indeed there is nearly no phase difference in span so no convection velocity is found. The convection in the spanwise direction is probably the key of the link between 2D and 3D buffet. There is a switch from 2D to 3D buffet only with the presence of this convection in span.

Buffet frequency strongly varies on the wing in the well-established regime while remaining more constant at onset and in deep buffet. The way it varies on the different models is almost the same: the frequency decreases towards the trailing edge, the same decreasing tendency is found in

the spanwise direction towards the wing tip. The Strouhal number values are consistent between the different models, the best way to compare the models is probably to use the local Strouhal number because of the different taper ratios between each model (0.83 for BUFET'N Co and 0.21 for FLIRET). A good agreement also is found considering MAC' as reference length. In this way the Strouhal numbers are in the same range of 0.2-0.3. Well defined as well is the decrease of the Strouhal number with α while the tendency with the Mach number is less clear and needs further study.

A convective behavior is found at buffet frequencies on the wing for all the models. The values of non-dimensional convective velocities are consistent between each other and a typical range of values $0.245 \pm 0.015 U_\infty$ could be defined. These values are smaller than the spanwise component of the freestream velocity ($U_\infty \sin(\Lambda) \approx 0.5 U_\infty$). Finally a spanwise convection of buffet cells is found (except for DTP Tremblement because unavailable), which confirms what has been observed in the literature [22]. This phenomenon has been presented in the introduction and it will be better analyzed in the next paragraph.

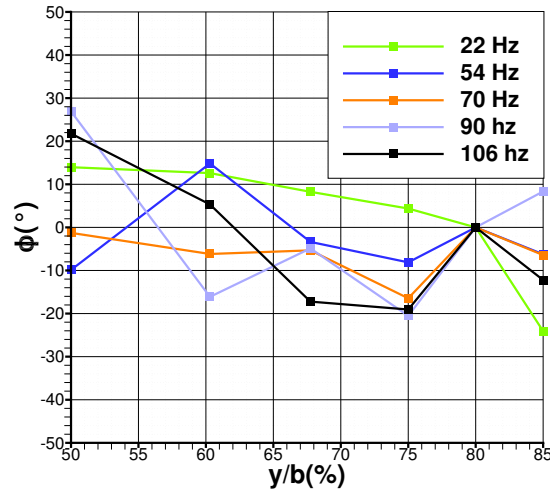


Fig. 21: Phase of cross-spectra at $x/c=85\%$ for two selected frequencies (reference sensor: $y/b=80\%$). AVERT test at $M=0.82$ and $\alpha=3^\circ$.

B. Prediction of buffet cells and 3D buffet model

The discovery of a convection phenomenon of cells in spanwise direction on a wing during buffet is very recent. As already said in the introduction, Iovnovich & Raveh [22] were the first to observe this convection numerically in 2015 and introduce the name of “buffet cells”. Dandois [14] found the convection on the AVERT project by using a cross-spectrum analysis. From the values of the phase difference it is possible to define the wavelength of the cells λ . For the AVERT project, two different values of λ/MAC are found: 1.3 for $\alpha = 4.25^\circ$ and 1.6 for $\alpha = 3.5^\circ$.

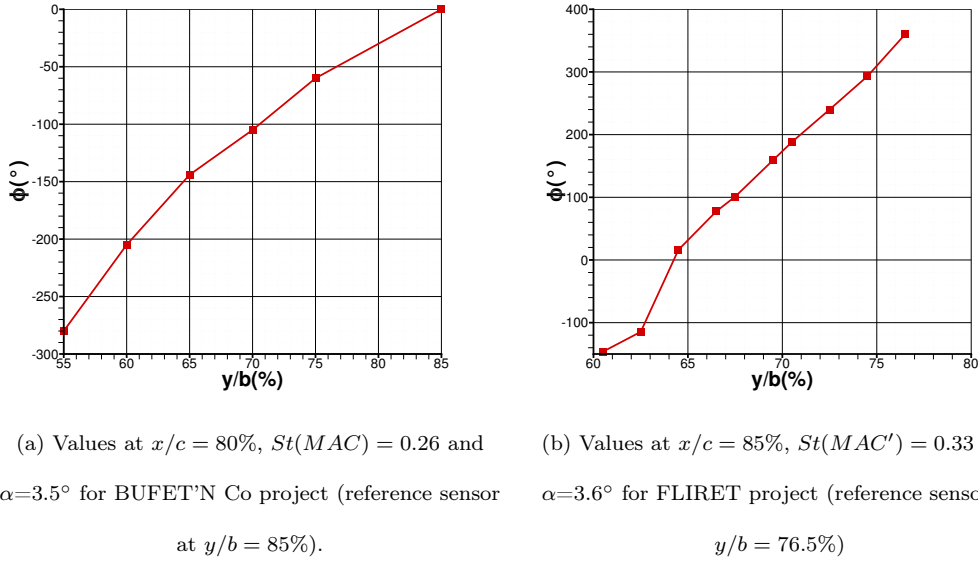


Fig. 22: Phase of cross-spectra along the span.

Figure 22 shows the phase differences in the spanwise direction for BUFET'N Co and FLIRET projects at the buffet frequencies. This information may then be translated into wavelengths characterizing the buffet cells $\lambda = U_C/f = 2\pi\Delta x/\Delta\phi$. Table 2 shows all the values of wavelengths computed and a comparison with the only value found in the literature. Wavelengths are presented here as non dimensional number, the reference lengths used being the same as the one used for the Strouhal number. It is possible to state that the wavelength decreases with the angle of attack but its precise value is strictly linked to the geometry of the wing, so it is not simple (probably not possible) to find out a unique value or a small range. FLIRET and BUFET'N Co are consistent with each other with values around 0.6; while the other two projects are more about 1.3. The value of

FLIRET increases if considering MAC' , so taking into account the geometry. But it is however not possible to compare the values of wavelengths from FLIRET (0.21 of taper ratio) with Iovnovich (1 of taper ratio). Even BUFET'N Co with a closer taper ratio (0.83) is not consistent with Iovnovich. Finally even if the geometrical dependency is very strong, it is still possible to define a range of wavelengths between 0.6 and 1.3 for these supercritical wings.

Table 2: Non dimensional wavelength for the convective buffets cells.

Projects:	AVERT	BUFET'N Co	FLIRET	Ref. [22] for $\Lambda = 30^\circ$
λ/MAC	1.3 at $\alpha=4.25^\circ$	0.56 at $\alpha=3.5^\circ$	0.62 at $\alpha=3.6^\circ$	1.3 at $\alpha=4^\circ$
	1.6 at $\alpha=3.5^\circ$		0.55 at $\alpha=3.8^\circ$	
λ/MAC'	1.6 at $\alpha=3.5^\circ$	0.56 at $\alpha=3.5^\circ$	0.9 at $\alpha=3.6^\circ$	1.3 at $\alpha=4^\circ$
λ/c (at $y/b = 78\%$)	1.9 at $\alpha=3.5^\circ$	1.25 at $\alpha=3.5^\circ$	1.2 at $\alpha=3.5^\circ$	1.3 at $\alpha=4^\circ$

To conclude this overview, figure 23 shows a sketch of the buffet cells convection over the FLIRET model. The value of wavelength and Strouhal are presented with MAC' as reference length together with the buffet convection velocity.

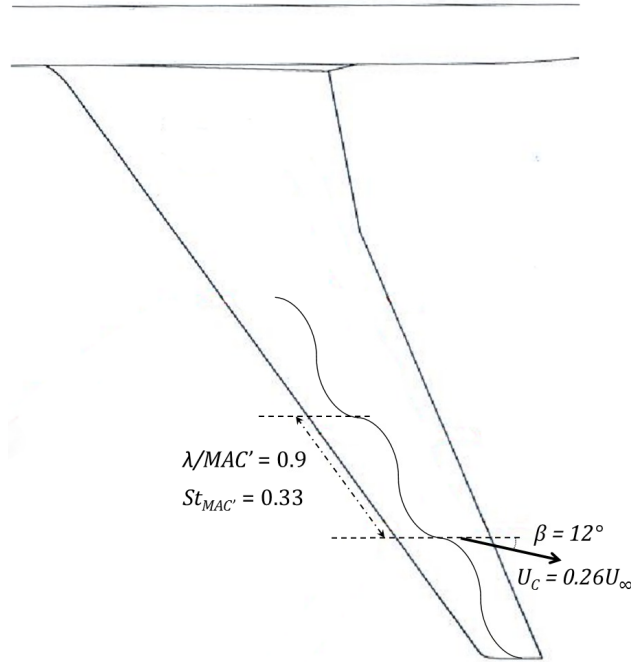


Fig. 23: Buffet cells convection on FLIRET model at $\alpha = 3.6^\circ$ and $M=0.85$.

VII. Conclusions and perspectives

There are two main results from the present study. The first is the characterization of all the convection velocities of the different phenomena propagating on the suction side of four different wings. This work shows that buffet is a strongly convective phenomenon in 3D and the values found are consistent for the different models so these values can be considered as typical of the phenomenon (for the sweep angle considered here). A decrease in the magnitude of the convective velocity is found when increasing α . It has been shown that these velocities are the main cause of a phenomenon of buffet cells convecting in the spanwise direction.

The second main result is the definition of a Strouhal number range of the phenomenon. It is important to underline the difference with [14] (of which this article is the continuation). Here the analysis is more oriented towards the variability of the phenomenon in the different projects and its sensibility with respect to the different configurations. Finally a range of Strouhal number based on the local chord of 0.2-0.3 is found.

At this point a comparison with the 2D transonic buffet is compulsory. The increase of the frequency (ref. [22] clearly showed its increase with the sweep angle), the change of shock amplitude oscillation and the creation of buffet cells are not still completely understood but the convection of buffet cells in the spanwise direction of the wing is the main difference between the two kinds of buffet. It is crucial in 3D to look for the unstable global mode found first by Crouch [6] in 2D. Indeed the spanwise convective nature of the 3D transonic buffet does not rule out the possibility of explaining it with a global mode as in 2D. If such a scenario is confirmed the two buffet would turn out to be very similar. The second hypothesis is a convective instability where the convection velocities wipe out the presence of an unstable global mode and establish a noise-amplifier behavior. A challenging 3D global stability analysis could state which hypothesis is more close to 3D transonic buffet. The only 3D global analysis performed until now by Timme & Thormann [10] does not really answer the question. Indeed the analysis has been performed only at low value of α and just the emergence of some destabilising global modes approaching the imaginary axis is found. Repeating the 3D global stability analysis with this point of view is a future main goal.

Acknowledgments

The AVERT S2MA wind tunnel tests were conducted within the FP7 AVERT European project (Contract No. AST5-CT-2006-030914), funded by the European Commission and project partners (Airbus Operations Ltd., Airbus Operations SL, Dassault Aviation, Alenia Aeronautica and Onera). The S3Ch wind tunnel tests have been performed in the framework of the ONERA's joint research project BUFET'N Co. devoted to "Buffet control on a transonic 3D wing using a closed-loop approach". The ETW wind tunnel tests were conducted within the FP6 FLIRET European project (Contract No. AIP3-CT-2003-502773), funded by the European Commission. Concerning the DTP Tremblement project, the authors gratefully acknowledge the DGAC from the French Ministry of Transport which granted the research reported in this paper.

- [1] B.H.K. Lee. Oscillatory shock motion caused by transonic shock boundary-layer interaction. *AIAA Journal*, 28(5):942–944, 1990. DOI: 10.2514/3.25144.
- [2] S. Deck. Numerical simulation of transonic buffet over a supercritical airfoil. *AIAA Journal*, 43(7):1556–1566, 2005. DOI: 10.2514/1.9885.
- [3] A. Memmolo, M. Bernardini, and S. Pirozzoli. Scrutiny of buffet mechanisms in transonic flow. *51st 3AF Int. Conference on Applied Aerodynamics*, FP43-2016, Strasbourg, France, 4-6 April 2016.
- [4] Q. Xiao, H.M. Tsai, and F. Liu. Numerical study of transonic buffet on a supercritical airfoil. *AIAA Journal*, 44(3):620–628, 2006. DOI: 10.2514/6.2004-1056.
- [5] L. Jacquin, P. Molton, S. Deck, B. Maury, and D. Soulevant. Experimental study of shock oscillation over a transonic supercritical profile. *AIAA Journal*, 47(9):1985 – 94, DOI: 10.2514/1.30190, 2009. DOI: 10.2514/1.30190.
- [6] J.D. Crouch, A. Garbaruk, and D. Magidov. Predicting the onset of flow unsteadiness based on global instability. *J. Comp. Phys.*, 224(2):924–940, 2007. DOI: 10.1016/j.jcp.2006.10.035.
- [7] J.D. Crouch, A. Garbaruk, D. Magidov, and A. Travin. Origin and structure of transonic buffet on airfoils. *J. Fluid Mech*, 628:pp. 357–369, 2009. DOI: 10.2514/6.2008-4233.
- [8] F. Sartor, C. Mettot, and D. Sipp. Stability, receptivity, and sensitivity analyses of buffeting transonic flow over a profile. *AIAA Journal*, 53(7):1980–1993, 2014. DOI: 10.2514/1.J053588.
- [9] F. Guiho. *Analyse de stabilité linéaire globale d’écoulements compressibles: application aux interactions onde de choc/couche limite*. PhD thesis, Paris, ENSAM, 2015.
- [10] S. Timme and R. Thormann. Towards three-dimensional global stability analysis of transonic shock buffet. *AIAA Atmospheric Flight Mechanics Conference*, AIAA Paper 2016-3848, 2016.
- [11] J. Reneaux, V. Brunet, D. Caruana, S. Deck, and P. Naudin. A combined experimental and numerical investigation of the buffet phenomenon and its control through passive and active devices. *CEAS Katnet Conference on Key Aerodynamic Technologies*, Bremen, Germany, 20-22 June 2005.
- [12] F.W. Roos. The buffeting pressure field of a high-aspect-ratio swept wing. *18th Fluid Dynamics and Plasma dynamics and Lasers Conference*, AIAA Paper 1985-1609, Cincinnati, OH, 16-18 July, 1985.
- [13] P. Molton, J. Dandois, A. Lepage, V. Brunet, and R. Bur. Control of buffet phenomenon on a transonic swept wing. *AIAA Journal*, 51(4):761–772, DOI: 10.2514/1.J051000, 2013. DOI: 10.2514/1.J051000.
- [14] J. Dandois. Experimental study of transonic buffet phenomenon on a 3D swept wing. *Phys. Fluids*, 28(1), 2016. DOI: 10.1063/1.4937426.
- [15] C. Hwang and W.S. Pi. Northrop F-5A aircraft transonic buffet pressure data acquisition and response analysis. *Journal of Aircraft*, 12(9):714–720, 1975. DOI: 10.2514/3.44487.

- [16] C. V. Eckstrom, D. A. Seidel, and M. C. Sandford. Unsteady pressure and structural response measurements on an elasticsupercritical wing. *Journal of Aircraft*, 27(1):75–80, 1990. DOI: 10.2514/3.44487.
- [17] R. Destuynder. Active control of the buffeting response on a large modern civil airplane configuration in wind tunnel. *2nd IFASD Conference*, Aachen, 1-3 April, 1985.
- [18] C. V. Eckstrom, D. A. Seidel, and M. C. Sandford. Measurements of unsteady pressure and structural response for an elastic supercritical wing. *NASA Technical Paper 3443*, 1994.
- [19] T. Lutz, P. P. Gansel, A. Waldmann, D.M. Zimmermann, and S. Schulte am Hülse. Prediction and measurement of the common research model wake at stall conditions. *Journal of Aircraft*, 53(2):501–514, 2015. DOI: 10.1098/rsta.2013.0325.
- [20] S. Deck, F. Gand, V. Brunet, and S. B. Khelil. High-fidelity simulations of unsteady civil aircraft aerodynamics: stakes and perspectives. application of zonal detached eddy simulation. *Phil. Trans. R. Soc. A*, 372(2022):1–21, 2014. DOI: 10.1098/rsta.2013.0325.
- [21] F. Sartor and S. Timme. Reynolds-Averaged Navier-Stokes simulations of shock buffet on half wing-body configuration. *53rd AIAA Aerospace Sciences Meeting*, AIAA Paper 2015-1939, 2015. DOI: 10.2514/6.2015-1939.
- [22] M. Iovnovich and D. E. Raveh. Numerical study of shock buffet on three-dimensional wings. *AIAA Journal*, 53(2):449 – 463, 2015. DOI: 10.2514/1.J053201.
- [23] V. Brunet and S. Deck. Zonal-detached eddy simulation of transonic buffet on a civil aircraft type configuration. *38th Fluid Dynamics Conference and Exhibit*, AIAA Paper 2008-4152, 2008. DOI:10.2514/6.2008-4152.
- [24] F. Sartor and S. Timme. Delayed detached-eddy simulation of shock buffet on half wing-body configuration. *22nd AIAA Computational Fluid Dynamics Conference*, AIAA Paper 2015-2607, 2015. DOI: 10.2514/6.2015-2607.
- [25] P. Huerre and M. Rossi. Hydrodynamic instabilities in open flows. *Collection alea saclay monographs and texts in statistical physics*, 1(3):81–294, 1998.
- [26] L. Larchevêque. *Simulation des grandes échelles de l'écoulement au-dessus d'une cavité*. PhD thesis, Paris 6, 2003.
- [27] J. Dandois, E. Garnier, and P. Sagaut. Numerical simulation of active separation control by a synthetic jet. *J. Fluid Mech.*, 574:25–58, 2007. DOI: 10.1017/S0022112006003995.
- [28] L. Larchevêque, P. Sagaut, T.H. Le, and P. Comte. Large-eddy simulation of a compressible flow in a three-dimensional open cavity at high reynolds number. *J. Fluid Mech.*, 516:265–301, 2004. DOI: 10.1017/S0022112004000709.